

Oscillations of solar atmosphere neutrinos

G. L. Fogli¹, E. Lisi¹, A. Mirizzi¹, D. Montanino² and P. D. Serpico³

¹*Dipartimento di Fisica and Sezione INFN di Bari, Via Amendola 173, 70126 Bari, Italy*

²*Dipartimento di Fisica and Sezione INFN di Lecce, Via Arnesano, 73100 Lecce, Italy*

³*Max-Planck-Institut für Physik (Werner-Heisenberg-Institut), Föhringer Ring 6, 80805 Munich, Germany*

The Sun is a source of high energy neutrinos ($E \gtrsim 10$ GeV) produced by cosmic ray interactions in the solar atmosphere. We study the impact of three-flavor oscillations (in vacuum and in matter) on solar atmosphere neutrinos, and calculate their observable fluxes at Earth, as well as their event rates in a kilometer-scale detector in water or ice. We find that peculiar three-flavor oscillation effects in matter, which can occur in the energy range probed by solar atmosphere neutrinos, are significantly suppressed by averaging over the production region and over the neutrino and antineutrino components. In particular, we find that the relation between the neutrino fluxes at the Sun and at the Earth can be approximately expressed in terms of phase-averaged “vacuum” oscillations, dominated by a single mixing parameter (the angle θ_{23}).

PACS numbers: 14.60.Pq, 96.50.Sb, 95.55.Vj, 26.65.+t

Preprint MPP-2006-92

I. INTRODUCTION

The Sun is a well-known source of low-energy electron neutrinos ($E \lesssim 20$ MeV), continually produced in its core by nuclear reactions. The study of this flux has been one of the most exciting enterprises in astroparticle physics, and has provided us with crucial evidence for ν flavor oscillations (see, e.g., [1, 2] and references therein).

High-energy neutrinos and antineutrinos (with $E \gtrsim 10$ GeV) are also continually produced by cosmic ray interactions in the solar atmosphere [3, 4, 5, 6, 7], which lead to the production of secondary mesons and their subsequent decay into ν_e , $\bar{\nu}_e$, ν_μ , and $\bar{\nu}_\mu$, collectively referred to as “solar atmosphere neutrinos” (SA ν) hereafter. From pion production dominance, at the source the SA ν flavor ratio is expected to be $\phi_e : \phi_\mu : \phi_\tau \simeq 1 : 2 : 0$, with approximately equal fluxes of ν and $\bar{\nu}$. Concerning the SA ν energy spectrum, the Monte Carlo simulation in [5] finds a power-law decrease ($\sim E^{-3}$) for $E \gtrsim 100$ GeV. At lower energies, heliomagnetic effects are expected to make the spectrum less steep (as $\sim E^{-2}$) [3, 6].

At the Earth, within the solid angle subtended by the Sun, the SA ν flux significantly exceeds the more familiar “atmospheric neutrino” flux generated by cosmic rays interacting with the Earth atmosphere. In fact, because of the different scale heights, the density at the first interaction point is lower in the solar atmosphere than in the terrestrial one, and therefore a larger fraction of mesons can decay into neutrinos instead of being absorbed. The expected SA ν signal can be quantified in terms of $O(10)$ events per year in a km^3 of water (or ice) above a threshold $E \gtrsim 100$ GeV [5], and might thus be detected by large-volume ν telescopes like IceCube [8].

The characterization of the SA ν signal is an important goal, both in itself and because it might represent a “background” in searches for signatures of possible weakly interacting massive particle (WIMP) annihilation in the Sun [9, 10, 11, 12, 13, 14, 15]. (Predicted

WIMP event rates are rather model-dependent, ranging from 10^{-12} to 10^3 events/year/ km^3 [15].)

Neutrino oscillations can significantly affect the SA ν flux, and must be taken into account in the calculation of the corresponding lepton event rates in detectors at the Earth. Earlier studies have stressed, e.g., the relevance of $\nu_\mu \rightarrow \nu_\tau$ vacuum oscillations [6], which might produce a few τ events per year in a km^3 detector (for $E > 100$ GeV), comparable to the τ event rate in OPERA, the CERN-to-Gran Sasso long-baseline experiment [16]. Although very challenging from an experimental viewpoint, the identification of SA ν -induced τ events in future ν telescopes might thus supplement laboratory tests of $\nu_\mu \rightarrow \nu_\tau$ appearance with their astrophysical counterpart. Given the potential importance of the SA ν signal detection, we think useful to revisit the impact of flavor transitions (in vacuum and in matter) on solar atmosphere neutrinos, in the light of the most recent advances in ν oscillation physics. In particular, taking into account updated values for the mass-mixing ν parameters, we investigate the three-flavor matter effects associated to SA ν propagation in the Sun.

The plan of our work is as follows. In Sec. II we describe the input SA ν fluxes at the Sun, basically taken from Refs. [5, 6]. In Sec. III we study SA ν oscillations in vacuum and matter within the standard 3ν mixing framework, and then calculate their flavor transition probabilities at Earth by solving numerically the flavor evolution equations. In Sec. IV we evaluate the impact of flavor oscillations on the observable events rates in a km^3 neutrino telescope. We summarize our results in Section V.

In a nutshell, we find that interesting, genuine three-flavor transitions in matter can take place during the SA ν propagation, but also that their impact is significantly suppressed by a “conspiracy” of various effects, including spatial and energy smearing, and $\nu/\bar{\nu}$ indistinguishability. In practice, the final oscillation effects can be approximated by (phase-averaged) vacuum flavor transitions, dominated by the mixing angle θ_{23} .

II. SOLAR ATMOSPHERE NEUTRINO FLUXES

Cosmic rays hitting the solar atmosphere produce secondary particles (mainly π 's, plus μ 's and K 's), which then produce both electron and muon neutrinos and antineutrinos¹ through their weak decay channels. The most recent calculation of the SA ν flux has been performed in [5] by using the Lund Monte Carlo programs PYTHIA and JETSET for high-energy particle interactions [17].

The fluxes at the source are approximately in the ratio

$$\phi_e : \phi_\mu : \phi_\tau \simeq 1 : 2 : 0 , \quad (1)$$

as expected by pion production dominance. Moreover, an almost equal number of ν and $\bar{\nu}$ is expected [5],

$$\nu : \bar{\nu} \simeq 1 : 1 . \quad (2)$$

After production, SA ν 's are affected by the solar medium through both absorption on nucleons and oscillations in matter. Absorption effects, which play a role only at energies $E \gtrsim 100$ GeV, depend on the impact parameter b of the neutrino trajectory,

$$0 \leq b \leq R_\odot , \quad (3)$$

where $b = 0$ corresponds to the Sun center, and $b = R_\odot (= 6.96 \times 10^5 \text{ km})$ to the solar disk border. In particular, for $E \sim 10^2\text{--}10^3$ GeV, a flux attenuation of $\mathcal{O}(10\%)$ or less is expected only for cases with $b \sim 0$ (which have little geometrical weight, since $> 50\%$ of the flux comes from $b > 0.7 R_\odot$), while for $E \gtrsim 10^3$ GeV absorption effects are sizable at any b [5]. For $E \gtrsim 100$ GeV, the approximate flavor-independence of the inelastic neutrino cross sections [13, 18] allows to factorize neutrino absorption from neutrino oscillation effects (which are, in principle, entangled) [19]. Therefore, in the energy range of interest for our work, absorption effects can be taken into account through an overall attenuation function multiplying the original ν fluxes [5], while oscillation effects can be applied afterwards.

We take the absorption-corrected, unoscillated fluxes of $\nu_e + \bar{\nu}_e$ and $\nu_\mu + \bar{\nu}_\mu$ from the parametrization in Eq. (15) of Ref. [5], which is integrated over the solar disk and is valid for neutrino energies $E > 100$ GeV. For $E < 100$ GeV, the only calculation of SA ν fluxes we are aware of is reported in [3], and depends appreciably on cosmic ray transport properties in the helio-magnetic fields. Following [6], we assume $\phi \propto E^{-\gamma}$, where γ is allowed to vary in the range $1.75 < \gamma < 2.45$ to parametrize helio-magnetic uncertainties.

In Figure 1 we show the unoscillated solar atmosphere ν fluxes at the Earth, based on the previous input choices.

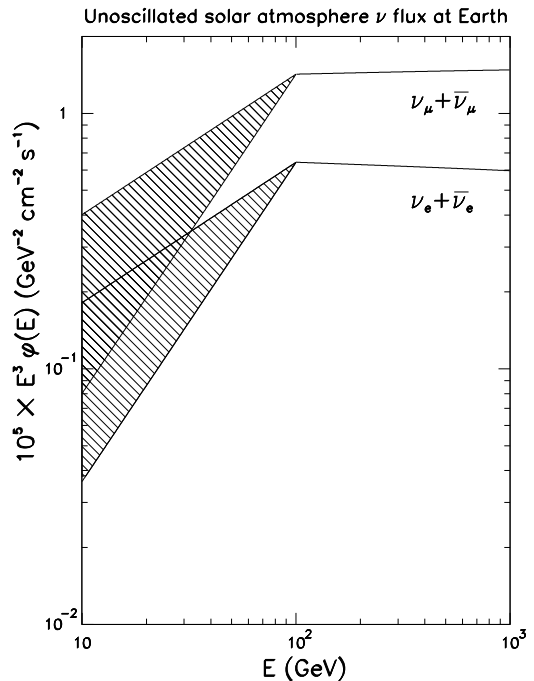


FIG. 1: Unoscillated fluxes of solar atmosphere neutrinos at the Earth in terms of neutrino energy. The fluxes are integrated over the Sun solid angle and summed over the ν and $\bar{\nu}$ components (basically equal). The dominant E^{-3} dependence is factorized out. For $E > 100$ GeV, the fluxes are taken from [5]. For $E < 100$ GeV, we take $\phi \propto E^{-\gamma}$ as in [6], with $1.75 < \gamma < 2.45$ (hatched areas). The overall normalization uncertainty (about 20%) is not shown.

A typical $\sim 20\%$ overall normalization error (not shown), due to primary cosmic ray flux uncertainties, should be added to the SA ν fluxes. The rapid decrease of the SA ν fluxes with energy is only partially compensated by the increase of the neutrino cross sections. Figure 2 shows the $\nu_\mu + \bar{\nu}_\mu$ flux (with an intermediate spectral index $\gamma = 2.1$ for $E < 100$ GeV) as well as the relevant charged-current interaction cross sections with the nucleons [18]. In the range $10 < E < 10^3$ GeV, the product $\phi \times \sigma$ decreases by more than three orders of magnitude, and thus the neutrino event rates above 1 TeV can be ignored in practice. For the same reason, relatively low experimental thresholds will be crucial for future SA ν detection.

A final technical comment is in order. We assume a b -independent flavor-ratio at the production, which is strictly true in the limit in which both pions and muons do not lose energy before decaying. We have verified the validity of this approximation for muons (for pions, given the similar mass but shorter lifetime, the approximation would be valid *a fortiori*). In particular, by using the solar atmosphere model reported in [5], we find that, in the “worst” case ($b \simeq 0$ and $E \simeq 1$ TeV), the muon range before decay is at least 20 times smaller than the typical stopping range for a TeV muon in hydrogen (or helium) [20]. We estimate that, for $E \lesssim 1$ TeV, the isotropic flavor-ratio limit is accurate to better than a few percent, in agreement with the results of Ref. [5].

¹ In the following, we shall sometimes loosely use the symbol “ ν ” to indicate both neutrinos and antineutrinos. When needed, a distinction between ν and $\bar{\nu}$ is made to avoid ambiguities.

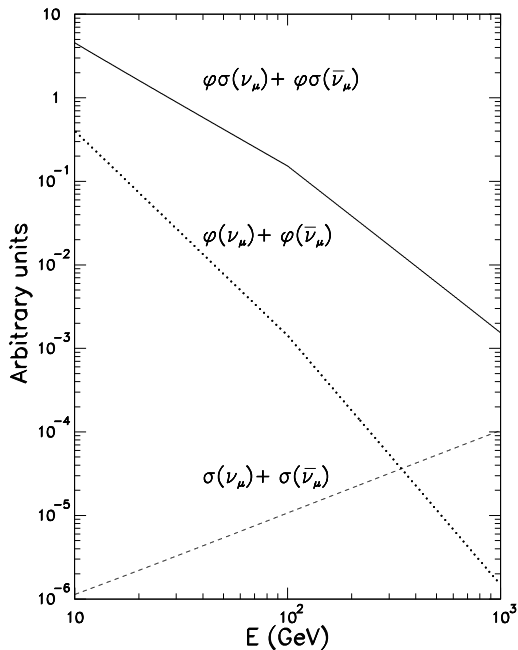


FIG. 2: Energy dependence of unoscillated SA ν fluxes (dotted line), of charged current interaction cross sections (dashed line), and of their product $\phi\sigma$ (thick solid line) for solar atmosphere $\nu_\mu + \bar{\nu}_\mu$, in arbitrary units. Curves for $\nu_e + \bar{\nu}_e$ (not shown) are very similar.

III. SOLAR ATMOSPHERE NEUTRINO OSCILLATIONS

Solar atmosphere neutrinos are affected by flavor oscillations (both in matter and in vacuum) during their propagation. Within the standard 3ν framework, the oscillation parameters include two squared mass differences (δm^2 , Δm^2) and three mixing angles (θ_{12} , θ_{23} , θ_{13}), whose ordered rotations form a unitary mixing matrix U . We take their best-fit values and 2σ ranges from [21]:

$$\delta m^2 = 7.92 (1 \pm 0.09) \times 10^{-5} \text{ eV}^2, \quad (4)$$

$$\Delta m^2 = 2.6 (1_{-0.15}^{+0.14}) \times 10^{-3} \text{ eV}^2, \quad (5)$$

$$\sin^2 \theta_{12} = 0.314 (1_{-0.15}^{+0.18}), \quad (6)$$

$$\sin^2 \theta_{23} = 0.45 (1_{-0.20}^{+0.35}), \quad (7)$$

$$\sin^2 \theta_{13} = (0.8_{-0.8}^{+2.3}) \times 10^{-2}. \quad (8)$$

The parameter Δm^2 has a physical sign, corresponding to the cases of normal hierarchy ($+\Delta m^2$) or inverted hierarchy ($-\Delta m^2$). In the following, unless otherwise specified, we assume normal mass hierarchy, and also set a possible CP-violating phase δ_{CP} to zero. Concerning the mixing parameter $\sin^2 \theta_{13}$, we shall use representative values below the current upper limits.

In matter, the ν oscillation dynamics also depends on the $\nu_e - \nu_{\mu,\tau}$ interaction energy difference V [22, 23],

$$\pm V(x) = \pm \sqrt{2} G_F N_e(x) \quad (+/- \text{ for } \nu/\bar{\nu}), \quad (9)$$

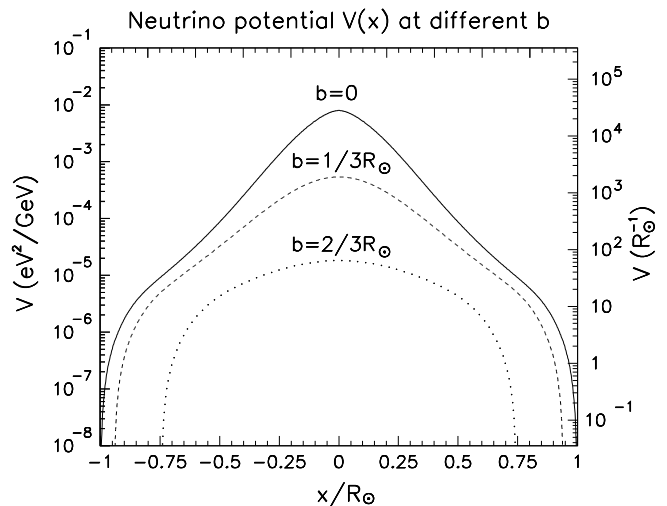


FIG. 3: Neutrino potential $V(x)$ in the Sun for three values of the impact parameter b . The ν trajectory coordinate x is normalized to the solar radius. The potential V is shown both in units of eV^2/GeV (left axis) and in units of inverse solar radius (right axis).

where N_e is the electron density, which we take from the standard solar model in [24], and x is the neutrino trajectory coordinate in the range $x \in [-x_{\text{max}}, +x_{\text{max}}]$, with $x_{\text{max}} = (R_\odot^2 - b^2)^{1/2}$. The effective potential V encountered by solar atmosphere neutrinos depends on the impact parameter $0 \leq b \leq R_\odot$. Figure 3 shows representative profiles of $V(x)$. Notice that the maximum of V decreases by almost three orders of magnitude as b increases from 0 to $2/3R_\odot$.

A. The “vacuum” approximation

Let us provisionally ignore matter effects by setting $V(x) = 0$ in the Sun (“vacuum” approximation, as studied in [6]). The oscillated SA ν fluxes at the detector D are given by

$$\phi_e^D = \phi_e P_{ee} + \phi_\mu P_{\mu e}, \quad (10)$$

$$\phi_\mu^D = \phi_e P_{e\mu} + \phi_\mu P_{\mu\mu}, \quad (11)$$

$$\phi_\tau^D = \phi_e P_{e\tau} + \phi_\mu P_{\mu\tau}, \quad (12)$$

where $P_{\alpha\beta} = P(\nu_\alpha \rightarrow \nu_\beta)$. The two independent vacuum neutrino oscillations wavelengths, given by $\lambda_L = 4\pi E/\delta m^2$ and $\lambda_H = 4\pi E/\Delta m^2$, read

$$\frac{\lambda_L}{R_\odot} = 4.51 \left(\frac{E}{100 \text{ GeV}} \right) \left(\frac{7.9 \times 10^{-5} \text{ eV}^2}{\delta m^2} \right), \quad (13)$$

$$\frac{\lambda_H}{R_\odot} = 0.14 \left(\frac{E}{100 \text{ GeV}} \right) \left(\frac{2.6 \times 10^{-3} \text{ eV}^2}{\Delta m^2} \right). \quad (14)$$

These wavelengths are typically much smaller than the Sun-Earth distance ($L \simeq 215 R_\odot$); indeed, in the worst

case ($E \simeq 1$ TeV) one has

$$L/\lambda_L \simeq 5 , \quad (15)$$

$$L/\lambda_H \simeq 150 . \quad (16)$$

The occurrence of many oscillation cycles in vacuum ($L/\lambda_{L,H} \gg 1$), smeared out by realistic energy resolution effects ($\Delta E/E \gtrsim 10\%$ is expected for km³-sized detectors [25]), guarantees the incoherence of the SA ν beam at the Earth (also when matter effects in the Sun are included, as done in the next Sections).

The vacuum oscillation probabilities are then given by their phase-averaged expressions,

$$P_{\alpha\beta}^{\text{vac}} = \sum_{i=1}^3 |U_{\alpha i}|^2 |U_{i\beta}|^2 . \quad (17)$$

If we further take $\sin^2 \theta_{13} \simeq 0$ (a reasonable approximation in the context of vacuum oscillations), then

$$P_{ee}^{\text{vac}} \simeq 1 - 2s_{12}^2 c_{12}^2 , \quad (18)$$

$$P_{e\mu}^{\text{vac}} \simeq 2c_{12}^2 s_{12}^2 c_{23}^2 , \quad (19)$$

$$P_{\mu\mu}^{\text{vac}} \simeq c_{23}^4 (1 - 2s_{12}^2 c_{12}^2) + s_{23}^4 , \quad (20)$$

$$P_{\mu\tau}^{\text{vac}} \simeq 2c_{23}^2 s_{23}^2 (1 - s_{12}^2 c_{12}^2) , \quad (21)$$

$$P_{e\tau}^{\text{vac}} \simeq 2c_{12}^2 s_{12}^2 s_{23}^2 , \quad (22)$$

where $c_{ij} \equiv \cos \theta_{ij}$ and $s_{ij} \equiv \sin \theta_{ij}$. For an initial flux ratio $\phi_e : \phi_\mu : \phi_\tau \simeq 1 : 2 : 0$, the oscillated fluxes at the detector read

$$\phi_e^D \simeq \phi_e [1 + 2c_{12}^2 s_{12}^2 (2c_{23}^2 - 1)] , \quad (23)$$

$$\phi_\mu^D \simeq \phi_\mu [1 - 2s_{23}^2 c_{23}^2 + s_{12}^2 c_{12}^2 c_{23}^2 (1 - 2c_{23}^2)] , \quad (24)$$

$$\phi_\tau^D \simeq \phi_\mu [2c_{23}^2 s_{23}^2 + c_{12}^2 s_{12}^2 s_{23}^2 (1 - 2c_{23}^2)] , \quad (25)$$

or, numerically,

$$\phi_e^D \simeq 1.043 \begin{pmatrix} +0.078 \\ -0.138 \end{pmatrix} \phi_e , \quad (26)$$

$$\phi_\mu^D \simeq 0.493 \begin{pmatrix} +0.050 \\ -0.001 \end{pmatrix} \phi_\mu , \quad (27)$$

$$\phi_\tau^D \simeq 0.485 \begin{pmatrix} +0.022 \\ -0.046 \end{pmatrix} \phi_\mu , \quad (28)$$

where the above central values are calculated for the best-fit values of s_{23}^2 and s_{12}^2 , while the (strongly asymmetric) errors are induced by the 2σ uncertainties of s_{23}^2 [see Eq. (7)]. This was recently noticed to be a common feature for several astrophysical neutrino sources [26, 27, 28]. The errors induced by the current uncertainties on s_{12}^2 and on s_{13}^2 are instead much smaller and can be neglected (see also Sec. III D below). For the specific case of 2-3 maximal mixing ($s_{23}^2 = 1/2$), one recovers a well-known result for the phase-averaged, vacuum neutrino flavor ratio at detection [29],

$$\phi_e^D : \phi_\mu^D : \phi_\tau^D \simeq 1 : 1 : 1 \text{ (max. mixing)} . \quad (29)$$

B. Matter effects

In the reference energy range $E \in [10, 1000]$ GeV, solar atmosphere neutrinos can actually experience peculiar three-flavor oscillation effects in matter which, in principle, may spoil the ‘‘vacuum’’ approximation discussed in the previous section. Matter effects introduce a characteristic refraction length $\lambda_r = 2\pi/V$, which can be expressed as

$$\frac{\lambda_r}{R_\odot} = 1.78 \times 10^{-6} \left(\frac{\text{eV}^2/\text{GeV}}{V} \right) . \quad (30)$$

In terms of λ_r , the oscillation wavelengths in matter read

$$\tilde{\lambda}_L = \frac{\lambda_L}{\sqrt{(\cos 2\theta_{12} \mp \lambda_L/\lambda_r)^2 + \sin^2 2\theta_{12}}} , \quad (31)$$

$$\tilde{\lambda}_H = \frac{\lambda_H}{\sqrt{(\cos 2\theta_{13} \mp \lambda_H/\lambda_r)^2 + \sin^2 2\theta_{13}}} , \quad (32)$$

where the $-(+)$ sign refers to neutrinos (antineutrinos).

Potentially large matter effects are expected when one of the above denominators is small, (‘‘resonance condition,’’ see [23]), i.e., roughly when

$$\lambda_{L,H} \sim \lambda_r . \quad (33)$$

In normal (inverted) hierarchy, the resonance conditions are realized only in the neutrino (antineutrino) channel. The fact that $\delta m^2 \ll \Delta m^2$ also implies that the conditions $\lambda_{L,H} \sim \lambda_r$ are realized at rather different energies. The dynamics of the 3ν system can then be often approximated in terms of two 2ν sub-systems, governed by (λ_L, θ_{12}) and (λ_H, θ_{13}) respectively.

At resonance, the oscillation lengths in matter are numerically given by

$$\frac{\tilde{\lambda}_L^{\text{res}}}{R_\odot} \simeq 0.97 \left(\frac{E}{20 \text{ GeV}} \right) \left(\frac{7.9 \times 10^{-5}}{\delta m^2/\text{eV}^2} \right) \left(\frac{0.93}{\sin 2\theta_{12}} \right) , \quad (34)$$

$$\frac{\tilde{\lambda}_H^{\text{res}}}{R_\odot} \simeq 0.68 \left(\frac{E}{100 \text{ GeV}} \right) \left(\frac{2.6 \times 10^{-3}}{\Delta m^2/\text{eV}^2} \right) \left(\frac{10^{-2}}{\sin^2 \theta_{13}} \right)^{\frac{1}{2}} , \quad (35)$$

the latter equation holding for small θ_{13} . Very different effects take place, when a resonance wavelength $\tilde{\lambda}^{\text{res}}$ is much smaller, comparable, or much larger than the solar radius R_\odot . For $\tilde{\lambda}^{\text{res}} \ll R_\odot$ (low-energy, adiabatic limit) one expects to recover the vacuum case with small, adiabatic matter corrections. For $\tilde{\lambda}^{\text{res}} \sim R_\odot$, the solar density profile structure is fully probed, and no particular approximation or limit is expected to work (also because the profile is non-monotonic, see Fig. 3); this situation is realized at $E \sim 20$ GeV (for $\tilde{\lambda}_L^{\text{res}}$) or at $E \sim O(10^2)$ GeV (for $\tilde{\lambda}_H^{\text{res}}$), see Eqs. (34, 35). Finally, for $\tilde{\lambda}^{\text{res}} \gg R_\odot$, one expects again to recover the vacuum limit but for a different reason: large wavelengths do not ‘‘resolve’’ the solar profile structure (extreme nonadiabatic limit [23]). In our

reference range $E \in [10, 1000]$ GeV, interesting matter effects are thus expected to emerge at different energies.

For $\theta_{13} = 0$ these effects are simplest to describe, since they are controlled only by (λ_L, θ_{12}) , and just one resonance condition ($\lambda_L \sim \lambda_r$) is effective. At low energy ($E \lesssim 10$ GeV), it is $\tilde{\lambda}_L^{\text{res}} \ll R_\odot$, and neutrinos oscillate many times in the solar matter, the phase information being lost. The potential changes slowly over one wavelength, so that the adiabatic approximation (no transition among mass eigenstates in matter) can be applied. The flavor transition probabilities are then given by $P_{\alpha\beta} = \sum_i |\tilde{U}_{\alpha i}|^2 |U_{i\beta}|^2$, where \tilde{U} is the mixing matrix in matter at the production point. However, since solar atmosphere neutrinos are produced in very low density regions, one can take $U \simeq \tilde{U}$ at the origin,² thus recovering the vacuum limit $P_{\alpha\beta} \simeq \sum_i |U_{\alpha i}|^2 |U_{i\beta}|^2$ at low energy ($E \lesssim 10$ GeV). At higher energies (say, $E \gtrsim 50$ GeV), it is instead $\tilde{\lambda}_L^{\text{res}} \gg R_\odot$: neutrino wavelengths can not resolve the details of the solar matter density profile, and the vacuum limit applies again [23]. In conclusion, for $\theta_{13} = 0$, significant matter effects are thus expected to emerge only around $E \sim \text{few} \times 10$ GeV.

For $\theta_{13} > 0$, one expects additional matter effects to occur besides the previous ones, since a second resonance condition ($\lambda_H \sim \lambda_r$) becomes effective. These effects, driven by (λ_H, θ_{13}) , are expected to build up at energies somewhat higher than for $\theta_{13} = 0$ [e.g., the relevant energy range is around $E \sim 100$ GeV for $s_{13}^2 \simeq 10^{-2}$, see Eq. (35)]. It should be noted that: (1) the two resonances, governed by different oscillation parameters, have different widths; (2) each is realized twice along the density profile (with partial cancellation effects); and (3) they may take place at energies not widely separated (e.g., 20 and 100 GeV), and thus may be partly entangled and non-factorizable. These complications prevent a straightforward generalization or construction of analytical recipes for calculations, in the spirit of those derived, e.g., in the context of solar neutrinos [30]. For this reason, in the following section we shall adopt numerical techniques in order to obtain quantitative results for the oscillation probabilities in the solar interior.

Finally, we mention that, in our reference energy range $E \in [10, 1000]$ GeV, possible matter effects in the Earth (before detection) are negligible, except perhaps at the lowest energies ($E \simeq 10\text{--}20$ GeV, see e.g. [31]), where they would be anyway much smaller than helio-magnetic flux systematics (see Fig. 1). For the specific case of IceCube, at the South Pole, neutrino trajectories in the Earth would also be relatively short. In conclusion, we can safely ignore Earth matter effects in the following.

C. Neutrino oscillation probabilities

To evaluate the SA ν oscillation probabilities $P_{\alpha\beta}$, we evolve numerically—through Runge-Kutta routines—the ν and $\bar{\nu}$ flavor evolution equations [23] for many different values of the impact parameter b , corresponding to different solar matter profiles (see Fig. 3). More precisely, we calculate first the amplitudes $A_\odot(\nu_\alpha \rightarrow \nu_i)$ from the production point to the Sun exit, where the ν_i 's are the mass eigenstates in vacuum. Then we obtain the flavor oscillation probabilities $P_{\alpha\beta}$ at the Earth as

$$P_{\alpha\beta} = \sum_{i=1}^3 |A_\odot(\nu_\alpha \rightarrow \nu_i)|^2 \cdot |U_{i\beta}|^2. \quad (36)$$

The above factorization of probabilities [23] from the production point to the Sun exit ($|A_\odot|^2$) and from the Sun exit to the detector at the Earth ($|U|^2$) is guaranteed by the suppression of all interference terms, due to the many oscillation cycles in vacuum and to the finite energy resolution.

From the unitarity property of the probabilities, one can express all the $P_{\alpha\beta}$'s in terms of only four independent quantities [12]. In the following, we choose P_{ee} , $P_{e\mu}$, $P_{\mu\mu}$ and $P_{\mu\tau}$ as independent set.

In Figure 4 we plot these probabilities as functions of neutrino energy E after gaussian energy resolution smearing (with $\Delta E/E = 10\%$ for definiteness), for a representative impact parameter $b = 1/3 R_\odot$, and for both $s_{13}^2 = 0$ (left panels) and $s_{13}^2 = 10^{-2}$ (right panels), assuming maximal 2-3 mixing and normal mass hierarchy in both cases. The upper and middle panels refer to neutrinos and antineutrinos, respectively. Since solar atmosphere ν 's and $\bar{\nu}$'s have approximately equal fluxes, and are basically indistinguishable in neutrino telescopes, we find it useful to plot the arithmetic average of the ν and $\bar{\nu}$ oscillation probabilities in the lower panels of Fig. 4.

For $\sin^2 \theta_{13} = 0$ (left panels of Fig. 4), the vacuum limit is reached for $E \gtrsim 50$ GeV, as discussed in the previous section. The same limit applies at very low energies ($E \lesssim 10$ GeV, not shown). In the vacuum limit, the probabilities $P_{\alpha\beta}$ are given by Eqs. (18–22), which numerically yield: $P_{ee} \simeq 0.57$, $P_{e\mu} \simeq 0.22$, $P_{\mu\mu} = P_{\mu\tau} \simeq 0.39$. Matter effects, as expected, emerge around $E \sim 20$ GeV, and are more pronounced in the neutrino channel (where the resonance condition $\lambda_L \sim \lambda_r$ can be realized). Notice that, at all energies, $P_{\mu\mu} = P_{\mu\tau}$. This is due to the fact that, for $\sin^2 \theta_{13} = 0$, $\nu_e \leftrightarrow \nu_{\mu,\tau}$ oscillations reduce to a pure two-family case (driven by δm^2 and θ_{12}), and the probabilities in matter can be expressed in terms of $P_{ee} = P_{ee}(\delta m^2, \theta_{12}, V)$ alone [31]. In particular, after phase averaging, one gets [32]

$$P_{\mu\mu} = s_{23}^4 + P_{ee} c_{23}^4, \quad (37)$$

$$P_{\mu\tau} = (1 + P_{ee}) s_{23}^2 c_{23}^2, \quad (38)$$

and thus $P_{\mu\mu} = P_{\mu\tau}$ for $s_{23}^2 = 1/2$. In addition, one gets $P_{e\mu} = (1 - P_{ee}) c_{23}^2$ [32], and thus “opposite” variations of $P_{e\mu}$ and P_{ee} , as evident in the left panels of Fig. 4.

² At typical SA ν production depths [$O(10^3)$ km], the density of the solar atmosphere is of $O(10^{-6})$ g cm $^{-3}$, and the neutrino potential is negligible for our purposes [$V \sim O(10^{-10})$ eV 2 /GeV, not even shown in Fig. 3]. Notice the difference with the more familiar adiabatic limit for solar neutrinos, where the high density at production (in the solar core) makes $\tilde{U} \neq U$.

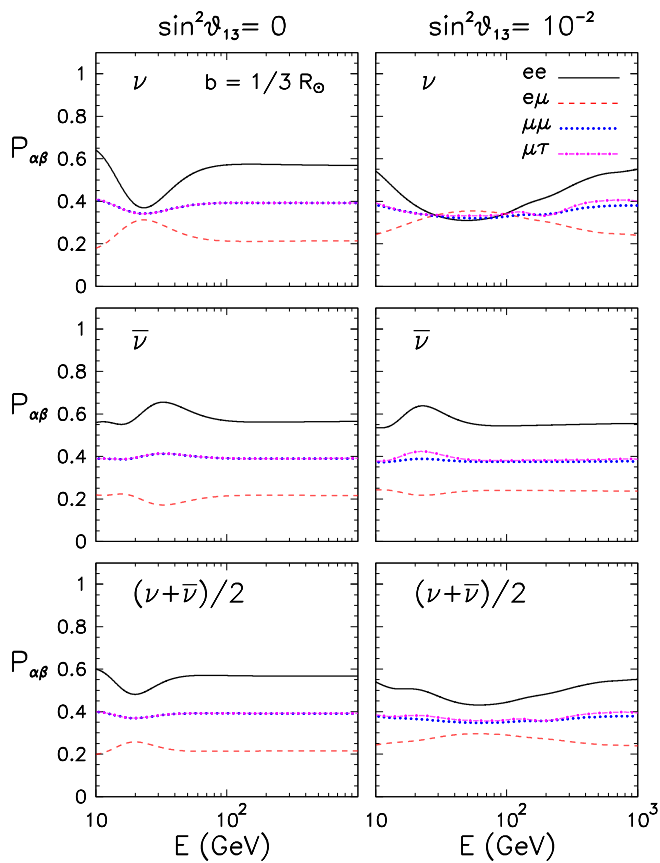


FIG. 4: Oscillation probabilities for solar atmosphere neutrinos as functions of energy, for $\sin^2 \theta_{13} = 0$ (left panels) and $\sin^2 \theta_{13} = 10^{-2}$ (right panels). We assume maximal 2-3 mixing, normal hierarchy and fix the impact parameter at $b = 1/3 R_{\odot}$. Probabilities are shown for ν (upper panels), $\bar{\nu}$ (middle panels), and their average $(\nu + \bar{\nu})/2$ (lower panels).

For $\sin^2 \theta_{13} = 10^{-2}$ (right panels of Fig. 4), additional three-flavor mixing effects, due to a second resonance, are seen to emerge in the neutrino channel around $E \sim 100$ GeV, with broad features entangled with the previous, lower resonance range. As compared with the left panels, the vacuum limit is reached at higher energies, but with almost the same limiting values for $P_{\alpha\beta}$. Most of the additional matter effects appear in ν_e -related oscillations, while $P_{\mu\mu}$ and $P_{\mu\tau}$ change little, the previous equality $P_{\mu\mu} = P_{\mu\tau}$ being only slightly perturbed.

The two lowest panels in Fig. 4 show that matter effects, averaged over ν and $\bar{\nu}$ components, produce only mild variations with respect to the vacuum limit, independently of the value of $\sin^2 \theta_{13}$. For inverted mass hierarchy, matter effects would be more prominent for antineutrino oscillation probabilities, but their average over ν and $\bar{\nu}$ would not be much different from Fig. 4. Therefore, even if we could select a specific solar atmosphere neutrino impact parameter b , the experimental $\nu/\bar{\nu}$ indistinguishability would make it hard to find signatures of matter effects, despite the fact that they may be potentially large on some $P_{\alpha\beta}$'s.

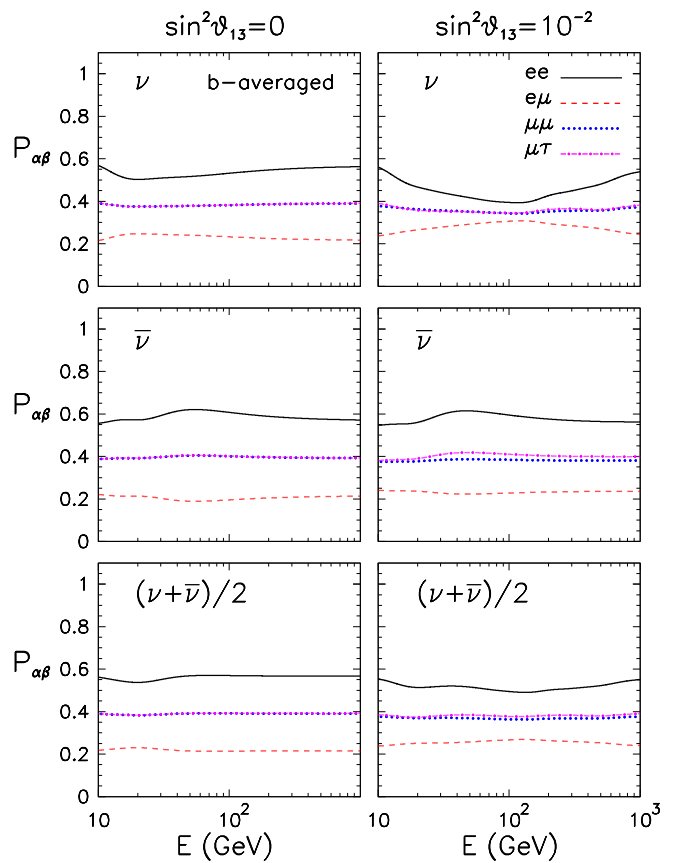


FIG. 5: Oscillation probabilities for solar atmosphere neutrinos, averaged over the impact parameter b , in the same format of Fig. 4.

Integration over the impact parameter b is expected to strengthen these conclusions, since trajectories with relatively high impact parameter b (and thus with short path in the Sun and small matter effects) have large geometrical weight. Indeed, given the limited angular resolution of neutrino telescopes ($\Delta\theta \gtrsim 1^\circ$ [25]), the solar disk angle ($\Delta\theta_{\text{sun}} \simeq 0.26^\circ$) cannot be resolved, and the neutrino oscillation probabilities must be averaged over b :

$$\langle P_{\alpha\beta}(E) \rangle = \frac{1}{\pi R_{\odot}^2} \int_0^{R_{\odot}} 2\pi b db P_{\alpha\beta}(E, b) . \quad (39)$$

Figure 5 shows the b -averaged oscillation probabilities, in the same format of Fig. 4. It appears that possible features associated to matter effects are strongly smeared out in the observable $\nu + \bar{\nu}$ channel. The energy dependence of all probabilities is rather flat and roughly insensitive to $\sin^2 \theta_{13}$, with only minor deviations from the vacuum limit governed by the parameter s_{23}^2 [Eqs. (18–22)]. Further considerations about realistic experimental conditions (integration above a given energy threshold, small expected statistics) can only strengthen such conclusions.

D. Variations of the oscillation parameters

The previous results show that observable SA ν flavor transition effects are dominated by the parameter $\sin^2 \theta_{23}$. Its relatively large experimental errors [Eq. (7)] represent, at present, the main uncertainty associated to oscillation effects in calculating both absolute and relative SA ν fluxes. In order to illustrate this point we choose a representative quantity which might be of interest in the future (should ν telescopes be able to discriminate electron events), namely, the electron-to-muon neutrino flux ratio at the detector.

Figure 6 shows the ϕ_e^D/ϕ_μ^D ratio (with fluxes summed over their ν and $\bar{\nu}$ components) as a function of the neutrino energy. The three oscillation parameters (Δm^2 , δm^2 , $\sin^2 \theta_{12}$) are fixed at their best-fit values, and normal hierarchy is assumed. The upper and lower sets of curves are obtained for the $\pm 2\sigma$ extremal values of $\sin^2 \theta_{23}$ from Eq. (7). Within each set of curves, $\sin^2 \theta_{13}$ is also taken at its $\pm 2\sigma$ extrema from Eq. (8), while the unknown phase δ_{CP} is set at either 0 or π (for $\sin^2 \theta_{13} \neq 0$). The spread of the curves due to the $\sin^2 \theta_{23}$ uncertainties amounts to about $\pm 15\%$, while the variations due to $(\sin^2 \theta_{23}, \delta)$ are roughly a factor three smaller. The $\pm 2\sigma$ errors of the other oscillation parameters (Δm^2 , δm^2 , $\sin^2 \theta_{12}$), as well as the change from normal to inverted hierarchy, would produce even smaller variations in the above curves (not shown). In practice, one can currently evaluate the effects of oscillation parameter uncertainties in terms of $\sin^2 \theta_{23}$ only. In the future, when $\sin^2 \theta_{23}$ will be determined much more accurately, one might need to account also for the (now subleading) errors of $(\sin^2 \theta_{13}, \delta_{CP})$. In the very far future, one might even hope that high-statistics samples of SA ν events could turn these effects from “uncertainties” to “observables.”

E. Summary of oscillation effects

We summarize this Section as follows. We have shown that solar atmosphere neutrinos are, in principle, subject to significant matter effects in the Sun, at least in some oscillation channels and for relatively central trajectories. These effects can be sensitive to θ_{13} and to both squared mass differences δm^2 and Δm^2 , as well as to the neutrino mass hierarchy and to δ_{CP} . However, by averaging over the neutrino and antineutrino channel, as well as over the impact parameter, these effects are significantly reduced.

For approximate estimates and for practical purposes, one can simply adopt the vacuum limit in Eqs. (18–22), and take into account only the uncertainties of θ_{23} (the spread of the other oscillation parameters being currently much less relevant). Numerically, one can take:

$$P_{ee} \simeq 0.57, \quad (40)$$

$$P_{e\mu} \simeq 0.43 c_{23}^2, \quad (41)$$

$$P_{\mu\mu} \simeq 0.57 c_{23}^4 + s_{23}^4, \quad (42)$$

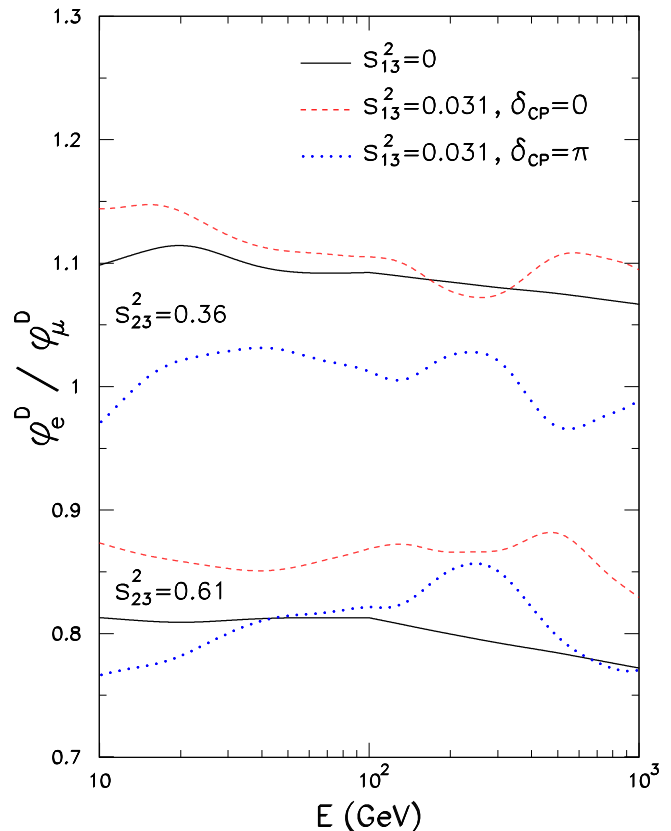


FIG. 6: Flux ratio ϕ_e^D/ϕ_μ^D as a function of energy, for normal hierarchy. The spread of the curves reflects the $\pm 2\sigma$ spread of $\sin^2 \theta_{23}$ and, to a lesser extent, of $\sin^2 \theta_{13}$ and δ_{CP} . The spread of the other oscillation parameters Δm^2 , δm^2 , and $\sin^2 \theta_{12}$ (here fixed to their best-fit values), as well as a change to inverted hierarchy, would produce only minor variations in the above curves (not shown).

$$P_{\mu\tau} \simeq 1.57 c_{23}^2 s_{23}^2, \quad (43)$$

$$P_{e\tau} \simeq 0.43 s_{23}^2, \quad (44)$$

where, currently, $s_{23}^2 \in [0.36, 0.61]$ at 2σ [Eq. (7)]. This amounts, e.g., to approximate the curves in the lower panels of Fig. 5 with flat, horizontal lines. Of course, when SA ν will be detected in future experiments, it will be worthwhile to make the best use of the data by fully including matter effects in the oscillation analysis, in order to avoid unnecessary approximations. For the sake of accuracy, we do include matter effects in the calculations discussed below.

IV. FLUXES AND EVENT RATES AT EARTH

Given the unoscillated input fluxes of Sec. II and the neutrino oscillation probabilities discussed in Sec. III, one can finally obtain the SA ν fluxes and event rates observable at the Earth. Figure 7 shows the oscillated $\nu_\mu + \bar{\nu}_\mu$ flux at the Earth, including matter effects (the results

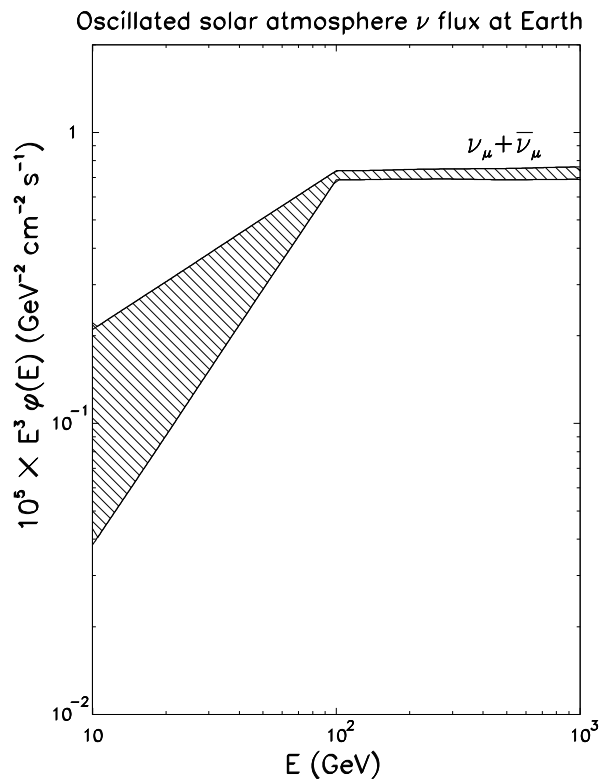


FIG. 7: Oscillated $\nu_\mu + \bar{\nu}_\mu$ flux of solar atmosphere neutrinos at the Earth, integrated over the solid angle of the Sun. The amplitude of the band above 100 GeV corresponds to the current $\pm 2\sigma$ uncertainties of the mixing parameter θ_{23} ; below 100 GeV, the dominant uncertainty is instead related to the energy spectral index.

with no matter effects would be, as already mentioned, very similar). The amplitude of the band in Fig. 7 includes the 2σ uncertainties in the mixing parameter θ_{23} from Eq. (7). Below ~ 100 GeV, it also includes the dominant uncertainty related to the energy spectral index γ . In particular, the upper curve in Fig. 7 is obtained for $s_{23}^2 = 0.61$ and $\gamma = 2.45$, while the lower curve is obtained for $s_{23}^2 = 0.36$ and spectral index $\gamma = 1.75$. The fluxes of $\nu_e + \bar{\nu}_e$ and $\nu_\tau + \bar{\nu}_\tau$ (not shown) would be very similar to the flux of $\nu_\mu + \bar{\nu}_\mu$, since the flavor ratio at the detection is roughly 1 : 1 : 1 around maximal mixing. To all such fluxes, one should add at least a $\sim 20\%$ normalization error (not shown) due to the uncertainties of the primary cosmic ray flux, and to the finite statistics of the flux simulations in [5].

Solar atmosphere neutrinos generate events observable in large-volume detectors above a certain energy threshold E_{th} . The corresponding event rates (for flavor α) are given by

$$R_\alpha = \int_{E_{\text{th}}}^{\infty} dE \phi_\alpha^D(E) \sigma_\alpha(E) \frac{\rho}{m_p} L_\alpha(E) A, \quad (45)$$

where ρ is the density of the medium ($\rho \simeq 1$ g/cm³ in water or ice), m_p is the proton mass (so that ρ/m_p is

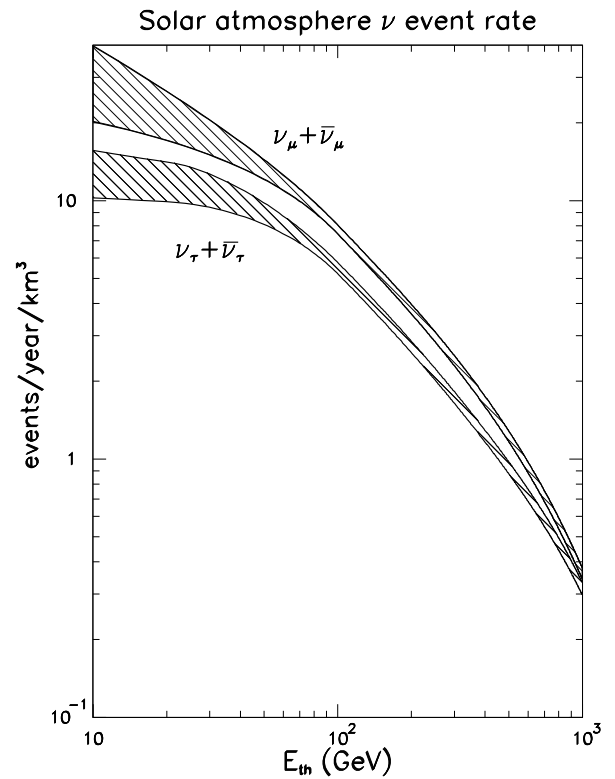


FIG. 8: ν_μ and ν_τ event rate in a km³ detector, as a function of the detector threshold energy E_{th} . The ν_e rate (not shown) is very similar to the one of ν_μ . The width of each band reflects the uncertainties on the initial fluxes and on the mixing parameters. See the text for details.

the target nucleon number density), σ_α is the cross section, $L_\alpha(E)$ is the range of the produced lepton (or the detector thickness h , whichever the larger), and A is the effective area of the detector. The charged-current interaction cross sections σ_α are taken from [18]. For an IceCube-like detector we take $A = 1$ km² and $h = 1$ km. Concerning the lepton range, we can take $L_e = h = L_\tau$, whereas for ν_μ

$$L_\mu(E) = \max \left\{ \frac{1}{\beta \rho} \ln \frac{E + \alpha/\beta}{E_{\text{th}} + \alpha/\beta}, h \right\}, \quad (46)$$

where the first term in brackets represents the distance travelled by a muon before its energy drops below the threshold E_{th} , the parameters $\alpha = 2.5$ MeV/(g cm⁻²) and $\beta = 4.0 \times 10^{-6}$ (g cm⁻²)⁻¹ being adopted from [5, 6]. More accurate calculations of the event rates would require MonteCarlo simulations for specific detector settings, which are beyond the scope of this work.

Figure 8 shows the results of our calculation for the muon and tau lepton event rates (summing over ν and $\bar{\nu}$), as functions of the threshold energy E_{th} , including oscillations in matter. (If the vacuum limit were adopted, the curves in Fig. 8 would change by $< 3\%$.) The rate of electron events (not shown) would be very similar to that of muon events. The width of the bands in Fig. 8 includes, as in Fig. 7, the uncertainties associated to s_{23}^2

and to γ . On top, one should add a systematic normalization uncertainty of $\sim \pm 20\%$ (not shown). It appears that a relatively low energy threshold (say, at or below 100 GeV) is crucial to get a handful of events per year in km-sized detectors. Note that the rate in Fig. 8 includes events from all arrival directions, both above the horizon (“downgoing”) and below the horizon (“upgoing”).

We conclude this Section with some qualitative remarks about future observations of solar atmosphere neutrino events with rates as low as those calculated in Fig. 8, which require careful background rejection.

The atmospheric neutrino background can be partly rejected by directional cuts (in the Sun’s direction). Unfortunately, the typical lepton scattering angle and detector angular resolution are larger than the solar disk angle. Therefore, despite the fact that the $SA\nu$ signal dominates over the atmospheric neutrino noise in the solar disk radius, the signal-to-background ratio drops to $\lesssim 1$ in realistic angular bins [6]. In addition, rejection of the muon background from cosmic rays showers (still huge at 10^2 – 10^3 GeV) requires the selection of upgoing events, with corresponding reduction of the event rates. However, even a few $SA\nu$ -induced muon events per year above a threshold of about 100 GeV (versus a prediction twice as large in the absence of θ_{23} -driven oscillations) might make it possible, in a decade or so, the “solar atmospheric neutrino check” of the large 2-3 mixing established by terrestrial atmospheric neutrinos.

When a $SA\nu$ signal will be established, a rough spectral analysis at different energy thresholds might also help to check the current expectations for energy spectral index. In this respect, our work clearly shows that neutrino oscillations cannot be responsible for dramatic variations of the $SA\nu$ rates with energy; if found, such variations should then be ascribed to other factors (e.g., unexpectedly large helio-magnetic effects above 100 GeV).

The uncertainties on the normalization and energy spectrum of the $SA\nu$ flux can also be reduced through solar gamma-ray data, since they have common production mechanisms (e.g., the γ ’s from π^0 decays). The upper limit sets by EGRET on the gamma flux above 100 MeV ($\Phi_\gamma < 2 \times 10^{-7}$ cm $^{-2}$ s $^{-1}$) [33] is only a factor ~ 3 above the nominal predictions of [3]. The galactic diffuse background in the same angular bin is about one order of magnitude smaller, and with the performances expected by the forthcoming GLAST satellite mission [34], the solar gamma signal should be easily detectable. This measurement may be complemented by the detection of the inverse Compton scattering photons produced by cosmic ray electrons, which probe the more external layers of solar atmosphere [35]. All in all, from gamma-ray astronomy we expect a relevant boost in the characterization of the solar heliosphere, with consequent sharpening of the predictions of $SA\nu$ fluxes.

Finally, let us briefly mention a technical point. Since the Sun works as a target for cosmic rays (thus generating $SA\nu$ ’s), it also shields the Earth from cosmic rays coming from the same solid angle (thus depleting atmospheric

ν ’s in that direction). One might then wonder whether, within the solar solid angle, the sought $SA\nu$ signal is accidentally compensated by the atmospheric ν depletion due to the Sun’s “shadow,” thus escaping detection. We argue that this is not the case, for at least two reasons: (i) the atmospheric ν background depletion is almost one order of magnitude smaller than the signal one is looking for; (ii) interplanetary magnetic fields displace (and smear) the Sun shadow. The exact displacement is difficult to predict, but the one measured with muons by MACRO [36] amounts to about 0.6° for median energies of the proton primaries of ~ 22 TeV. For the lower energies we are focusing on, we expect larger displacements, which may allow to separate the Sun shadow in the atmospheric ν background from the position of the $SA\nu$ excess. Finally, the position of this dip (and the similar one due to the Moon shadow) will be tagged more accurately in neutrino telescopes through downgoing muons, and thus the deficit should be easily corrected for.

V. CONCLUSIONS AND PROSPECTS

During the last forty years, the Sun has been the most important source of astrophysical neutrinos, which have provided us with crucial evidence of neutrino oscillations. Neutrino astrophysics is now entering a new era, where next generation neutrino telescopes will be capable to detect high-energy (extra)galactic astrophysical neutrino fluxes from new sources. These ν ’s would be useful both to probe the properties of the sources [37] and to test for new physics beyond the standard three-neutrino mixing scenario [38].

The same telescopes might be able to “see” the Sun in a new way, namely, as a source of high energy neutrinos, produced by cosmic ray interactions in the solar atmosphere ($SA\nu$). Even if only a handful of events per year may be detectable in a km 3 telescope, their theoretical fluxes are relatively under control, and thus a measurement might provide a high-energy, astrophysical probe of neutrino flavor mixing. Moreover, the $SA\nu$ flux represents an unavoidable background in searching possible neutrino fluxes induced by WIMP annihilation in the Sun core. For these reasons, it appears worthwhile to characterize the $SA\nu$ flux detectable at the Earth, after neutrino oscillations have occurred in the solar matter and in vacuum.

In our work we have studied solar atmosphere neutrino oscillations in detail, in the light of the most recent determinations of the neutrino mass mixing parameters, and paying particular attention to matter effects (generally neglected a priori in this context). We have found that, in the energy range $E \in [10, 1000]$ GeV relevant for detection, $SA\nu$ oscillations in matter have in principle a rich phenomenology, and can generate effects which depend on all 3ν mass-mixing parameters. Unfortunately, these effects are smeared out to a large extent by summing over the neutrino and antineutrino channel, and

by integrating over the solar disk angle (as well as over energy). In practice, oscillations are dominated by the “vacuum” effect of the θ_{23} mixing angle. Therefore, even if matter effects can and do occur, the original flavor ratio $\phi_e : \phi_\mu : \phi_\tau \simeq 1 : 2 : 0$ at the source approximately yields the well-known ratio $\phi_e^D : \phi_\mu^D : \phi_\tau^D \simeq 1 : 1 : 1$ at the detector (for maximal 2-3 mixing), just as in the case of phase-averaged vacuum oscillations.

Further refinements may include improved estimates of the input $\text{SA}\nu$ fluxes and of their uncertainties. In recent years, significant progress has been made in determining the cosmic ray composition and in refining the interaction and cascade development models [39]. More detailed solar atmosphere models [40] and future gamma ray data might also help to constrain the $\text{SA}\nu$ production mechanism. In particular, observations in gamma rays may sharpen our knowledge of helio-magnetic effects [3, 35]. Earlier estimates of the unoscillated $\text{SA}\nu$ fluxes [3, 4, 5, 6] could thus be usefully revisited. This task will certainly become mandatory if a $\text{SA}\nu$ signal will be found

in neutrino telescopes or, even better, if it will become a background for signatures of WIMP annihilation in the Sun.

Acknowledgments

We thank M. Maltoni and G. Sigl for useful comments. This work is supported in part by the Italian “Istituto Nazionale di Fisica Nucleare” (INFN) and by the “Ministero dell’Istruzione, Università e Ricerca” (MIUR) through the “Astroparticle Physics” research project. The work of P.D.S. is supported in part by the Deutsche Forschungsgemeinschaft under grant No. SFB 375 and by the European Union under the ILIAS project, contract No. RII3-CT-2004-506222. A.M. acknowledges kind hospitality at the Max-Planck-Institut für Physik (Munich, Germany), where this work was completed.

-
- [1] J.N. Bahcall, *Neutrino Astrophysics* (Cambridge U. Press, Cambridge, England, 1989).
- [2] G. L. Fogli, E. Lisi, A. Marrone and A. Palazzo, “Solar neutrinos (with a tribute to John N. Bahcall),” Proceedings of *NO-VE 2006*, 3rd International Workshop on Neutrino Oscillations in Venice (Venice, Italy, 2006), ed. by Milla Baldo Ceolin (Edizioni Papergraf, Padova, Italy, 2006), p. 69 [hep-ph/0605186].
- [3] D. Seckel, T. Stanev, and T. K. Gaisser, “Signatures of cosmic-ray interactions on the solar surface,” *Astrophys. J.* **382**, 652 (1991).
- [4] I. V. Moskalenko and S. Karakula, “Very high-energy neutrinos from the sun,” *J. Phys. G* **19**, 1399 (1993).
- [5] G. Ingelman and M. Thunman, “High Energy Neutrino Production by Cosmic Ray Interactions in the Sun,” *Phys. Rev. D* **54**, 4385 (1996) [hep-ph/9604288].
- [6] C. Hettlage, K. Mannheim and J. G. Learned, “The sun as a high energy neutrino source,” *Astropart. Phys.* **13**, 45 (2000) [astro-ph/9910208].
- [7] J. G. Learned and K. Mannheim, “High-energy neutrino astrophysics,” *Ann. Rev. Nucl. Part. Sci.* **50**, 679 (2000).
- [8] F. Halzen, “Astroparticle physics with high energy neutrinos: From AMANDA to IceCube,” astro-ph/0602132.
- [9] M. Srednicki, K. A. Olive and J. Silk, “High-energy neutrinos from the Sun and cold dark matter,” *Nucl. Phys. B* **279**, 804 (1987).
- [10] J. R. Ellis, R. A. Flores and S. S. Masood, “MSW effect on high-energy solar neutrinos from relic annihilation,” *Phys. Lett. B* **294**, 229 (1992).
- [11] L. Bergstrom, J. Edsjo and P. Gondolo, “Indirect detection of dark matter in km-size neutrino telescopes,” *Phys. Rev. D* **58**, 103519 (1998) [hep-ph/9806293].
- [12] A. de Gouvea, “The oscillation probability of GeV solar neutrinos of all active species,” *Phys. Rev. D* **63**, 093003 (2001) [hep-ph/0006157].
- [13] P. Crotty, “High-energy neutrino fluxes from supermassive dark matter,” *Phys. Rev. D* **66**, 063504 (2002) [hep-ph/0205116].
- [14] M. Cirelli *et al.*, “Spectra of neutrinos from dark matter annihilations,” *Nucl. Phys. B* **727**, 99 (2005) [hep-ph/0506298].
- [15] F. Halzen and D. Hooper, “Prospects for detecting dark matter with neutrino telescopes in light of recent results from direct detection experiments,” *Phys. Rev. D* **73**, 123507 (2006) [hep-ph/0510048].
- [16] C. Sirignano for the OPERA Collaboration, “The CNGS project and OPERA experiment at LNGS,” talk at *Neutrino 2006*, 22nd International Conference on Neutrino Physics and Astrophysics, available at: neutrinosantafe06.com.
- [17] T. Sjostrand, “PYTHIA 5.7 and JETSET 7.4: Physics and manual,” *Comput. Phys. Commun.* **82**, 74 (1994) [hep-ph/9508391].
- [18] R. Gandhi, C. Quigg, M. H. Reno and I. Sarcevic, “Neutrino interactions at ultrahigh energies,” *Phys. Rev. D* **58**, 093009 (1998) [hep-ph/9807264]; S. Dutta, R. Gandhi and B. Mukhopadhyaya, “Tau-neutrino appearance searches using neutrino beams from muon storage rings,” *Eur. Phys. J. C* **18**, 405 (2000) [hep-ph/9905475].
- [19] V. A. Naumov, “High-energy neutrino oscillations in absorbing matter,” *Phys. Lett. B* **529**, 199 (2002) [hep-ph/0112249].
- [20] D. E. Groom, N. V. Mokhov and S. I. Striganov, “Muon stopping power and range tables 10-MeV to 100-TeV,” *Atom. Data Nucl. Data Tabl.* **78**, 183 (2001).
- [21] G. L. Fogli *et al.*, “Observables sensitive to absolute neutrino masses: A reappraisal after WMAP-3y and first MINOS results,” [hep-ph/0608060]; see also: G. L. Fogli, E. Lisi, A. Marrone and A. Palazzo, “Global analysis of three-flavor neutrino masses and mixings,” *Prog. Part. Nucl. Phys.* **57**, 742 (2006) [hep-ph/0506083].
- [22] L. Wolfenstein, “Neutrino Oscillations In Matter,” *Phys. Rev. D* **17**, 2369 (1978); S. P. Mikheev and A. Yu. Smirnov, “Resonance Enhancement Of Oscillations In Matter And Solar Neutrino Spectroscopy,” *Yad. Fiz.* **42**,

- 1441 (1985) [Sov. J. Nucl. Phys. **42**, 913 (1985)].
- [23] T. K. Kuo and J. T. Pantaleone, “Neutrino Oscillations In Matter,” *Rev. Mod. Phys.* **61**, 937 (1989).
- [24] J. N. Bahcall, A. M. Serenelli and S. Basu, “New solar opacities, abundances, helioseismology, and neutrino fluxes,” *Astrophys. J.* **621**, L85 (2005) [astro-ph/0412440].
- [25] J. F. Beacom *et al.*, “Measuring flavor ratios of high-energy astrophysical neutrinos,” *Phys. Rev. D* **68**, 093005 (2003) [Erratum-ibid. *D* **72**, 019901 (2005)] [hep-ph/0307025].
- [26] P. D. Serpico, “Probing the 2-3 leptonic mixing at high-energy neutrino telescopes,” *Phys. Rev. D* **73**, 047301 (2006) [hep-ph/0511313].
- [27] P. D. Serpico and M. Kachelrieß, “Measuring the 13-mixing angle and the CP phase with neutrino telescopes,” *Phys. Rev. Lett.* **94**, 211102 (2005) [hep-ph/0502088].
- [28] M. Kachelriess and R. Tomas, “High energy neutrino yields from astrophysical sources. I: Weakly magnetized sources,” *Phys. Rev. D* **74**, 063009 (2006) [astro-ph/0606406].
- [29] H. Athar, M. Jezabek and O. Yasuda, “Effects of neutrino mixing on high-energy cosmic neutrino flux,” *Phys. Rev. D* **62**, 103007 (2000) [hep-ph/0005104].
- [30] G. L. Fogli, E. Lisi, D. Montanino and A. Palazzo, “Quasi-vacuum solar neutrino oscillations,” *Phys. Rev. D* **62**, 113004 (2000) [hep-ph/0005261]; E. Lisi *et al.*, “Analytical description of quasivacuum oscillations of solar neutrinos,” *Phys. Rev. D* **63**, 093002 (2001) [hep-ph/0011306].
- [31] E. K. Akhmedov, M. Maltoni and A. Y. Smirnov, “Describing oscillations of high energy neutrinos in matter precisely,” *Phys. Rev. Lett.* **95**, 211801 (2005) [hep-ph/0506064].
- [32] O. L. G. Peres and A. Yu. Smirnov, “Testing the solar neutrino conversion with atmospheric neutrinos,” *Phys. Lett. B* **456**, 204 (1999) [hep-ph/9902312].
- [33] D. J. Thompson, D. L. Bertsch, D. J. Morris and R. Mukherjee, “Energetic gamma ray experiment telescope high-energy gamma ray observations of the Moon and quiet Sun,” *Journal of Geophys. Res.* **102** (A7), 14735 (1997).
- [34] See the website: www-glast.slac.stanford.edu
- [35] I. V. Moskaleenko, T. A. Porter and S. W. Digel, “Inverse Compton scattering on solar photons, heliospheric modulation, and neutrino astrophysics,” *Astrophys. J. Letters*, in press [astro-ph/0607521].
- [36] M. Ambrosio *et al.* [MACRO Collaboration], “Moon and sun shadowing effect in the MACRO detector,” *Astropart. Phys.* **20**, 145 (2003) [astro-ph/0302586].
- [37] G. Barenboim and C. Quigg, “Neutrino observatories can characterize cosmic sources and neutrino properties,” *Phys. Rev. D* **67**, 073024 (2003) [hep-ph/0301220].
- [38] J. F. Beacom *et al.*, “Decay of high-energy astrophysical neutrinos,” *Phys. Rev. Lett.* **90**, 181301 (2003) [hep-ph/0211305]; J. F. Beacom *et al.*, “Pseudo-Dirac neutrinos, a challenge for neutrino telescopes,” *Phys. Rev. Lett.* **92**, 011101 (2004) [hep-ph/0307151]; D. Hooper, D. Morgan and E. Winstanley, “Lorentz and CPT invariance violation in high-energy neutrinos,” *Phys. Rev. D* **72**, 065009 (2005) [hep-ph/0506091].
- [39] T. Stanev, *High Energy Cosmic Rays* (Springer-Praxis, Berlin, 2004).
- [40] Y. Gu *et al.*, “A Stochastic Model of the Solar Atmosphere,” *Astrophys. J.* **484**, 960 (1997).